Composite Structures 372 (2025) 119500

Contents lists available at ScienceDirect

Composite Structures

journal homepage: www.elsevier.com/locate/compstruct

A composite gradient index lens for wideband elastic waves focusing: Design approach and experimental validation at constant thickness

Valentin Rapine [a,*], Nour Abuhemeida [b], Morvan Ouisse [b], Scott Cogan [b], Pascal Francescato [a], Rémy Lachat [c], Yann Meyer [a]

[a] Université Savoie Mont-Blanc, SYMME, Annecy, 74000, France
[b] SUPMICROTECH, Université de Franche-Comté, CNRS, Institut Femto-ST, Besançon, F-25000, France
[c] UTBM, CNRS, Laboratoire Interdisciplinaire Carnot de Bourgogne ICB UMR 6303, Belfort, F-90010, France

ARTICLE INFO

Keywords:
Elastics waves
Grin-lens
Focusing
Energy harvesting
Layered structure
Mechanical properties

ABSTRACT

Vibrational energy focusing is of significant interest in fields such as energy harvesting, particularly with the emergence of smart structures and self-powered technologies. This paper presents the design and manufacturing approach for Gradient-Index (GRIN) lenses using composite materials. As a proof of concept, the strategy implemented here focuses on controlling the fiber mass ratio of a unidirectional (UD) composite at constant thickness. Mechanical properties must be carefully controlled throughout a dedicated manufacturing process to achieve a gradient of phase velocity for focusing elastic flexural waves. Numerical calculation have demonstrated the efficiency of energy focusing within a frequency range from 2 kHz to 8 kHz. A manufacturing process has been developed to prototype a composite structure that integrates the designed GRIN lens. Additionally, the comparison of a numerical model with experimental results from a manufactured lens structure reveals that the energy density in a defined focusing zone can be increased sevenfold using a gradient lens composite structure, with an incident wave of 8 kHz.

1. Introduction

Mechanical parts such as aircraft wings, wind turbine blades operating in dynamic environments act as elastic media, where bending waves propagate during operation [1]. These waves carry valuable information about the structural health of the part and their energy could be used to power sensors and actuators [2,3]. By analyzing the vibratory behavior, it is possible to detect and localize damage, ensuring the reliability of the part during its lifespan. In the context of smart structures [4,5], where autonomous systems [6] aim to harvest energy from elastic deformations to power sensors or sensor networks, a significant challenge arises. The energy recovered from bending waves is often insufficient to sustain such systems. To address this, controlling the propagation of bending waves along preferential trajectories emerges as a critical solution. By directing these waves toward specific regions, their energy can be concentrated, maximizing the energy density in targeted zones and significantly enhancing the efficiency of energy harvesting mechanisms. By strategically concentrating bending wave energy in a defined zone, it also becomes possible to minimize vibratory energy in regions where it could cause unwanted effects, such as structural fatigue, noise, or interference with sensitive components. This approach is particularly relevant in applications where controlling vibrations is critical for maintaining operational integrity or ensuring the longevity of the system.

GRadient-INdex lenses (GRIN lenses) are systems with a gradient index of refraction allowing waves to focus. A specific variation of medium properties along the axis transverse to the propagation direction makes a phase velocity gradient to focus an incident plane wave. It was initially studied and developed in fields such as optics [7,8] with electromagnetic waves. Recently this phenomenon has a great interest in acoustic and elastic waves for energy harvesting [9–11]. For instance, it is a solution to capture, concentrate and extract more energy by placing a harvesting system on the focusing zone [12]. Phase velocity of elastic bending waves has different parameters of design: mass density, elasticity modulus and thickness. Therefore, several design strategies exploiting these parameters exist to manage the required gradient properties to focus elastic bending waves.

A specific thickness gradient with an isotropic material shows good results to focus elastic bending waves [10,12–15]. Another way to tailor phase velocity is a periodic array of shunted piezoelectric transducers with a specific impedance [16,17]. Numerous research investigate

* Corresponding author.
E-mail addresses: valentin.rapine@univ-smb.fr (V. Rapine), nour.abuhemeida@femto-st.fr (N. Abuhemeida), morvan.ouisse@femto-st.fr (M. Ouisse), scott.cogan@univ-fcomte.fr (S. Cogan), pascal.francescato@univ-smb.fr (P. Francescato), remy.lachat@utbm.fr (R. Lachat), yann.meyer@univ-smb.fr (Y. Meyer).

https://doi.org/10.1016/j.compstruct.2025.119500
Received 20 March 2025; Received in revised form 10 June 2025; Accepted 16 July 2025
Available online 5 August 2025

about periodic structures, phononic crystal [9,11,18–39] that exploit Bragg scattering to use wave interference. This solution necessitates that the dimensions of the periodic structure align closely with the wavelength. Moreover, another approach to focus energy instead of lens, uses phononic crystal to make Bragg mirror to concentrate energy [28,40,41]. Due to geometrical constraints and manufacturing complexity, these modulation strategies are difficult to reconcile with standard engineering requirements, which could restrict their applicability in conventional frameworks, depending on the specific design constraints and manufacturing capabilities.

Composites are key materials in many fields (transport, aeronautics, renewable energies, etc.). Their physical properties, particularly mechanical properties, can be tailored to best meet a given specification. The design freedoms offered by composite materials are of particular interest for GRIN lens design. A composite material is made up of several phases. In most cases, it is composed of two phases: the matrix (a polymer resin) and a reinforcement (unidirectional fibers, fabrics, etc.). The matrix holds the reinforcement to create the required shape, while the reinforcement increases mechanical characteristics of the matrix. It makes it possible to obtain local changes in properties (thickness, stiffness, density) that will influence the overall vibratory behavior of the structure. An important aspect to consider is that the refractive index is inherently linked to the material's thickness, stiffness, and density, providing flexibility in tailoring the design strategy to meet the part's overall specifications while minimizing the intrusive nature of a lens structure. For instance, in applications such as wind turbine blades or aircraft wings, the external geometry is critical for aerodynamic performance. In such cases, the gradient can be implemented by modifying the thickness internally, preserving the external shape. If internal thickness modifications are also constrained, alternative strategies can involve creating a gradient in stiffness and/or density to achieve the desired refractive index distribution. This adaptability ensures compatibility with the part's functional and structural requirements, while maintaining optimal performance. Composites structures offers several solutions to get the desired gradient. Considering the thickness constrained by general specification, the first is to use laminates to manage the homogenized modulus with different ply orientations. A second approach, adopted in this article as a proof of concept for experimental validation, involves the use of unidirectional layers at constant thickness, to achieve variations in stiffness and density. The more fibers there are in a given area, the greater the stiffness and the density of the composite. Therefore to obtain the stiffness and density required to reach the desired phase velocity, we manage the fiber-mass ratio of the composite materials in specified area. The aim is to find an operating point in a given design space, taking into account manufacturing constraints. In this context, using a plate as a simplified model to demonstrate the GRIN lens concept offers an effective proof of concept that can be generalized to more complex structures. Plates provide a straightforward design to isolate and study fundamental wave propagation phenomena. Moreover, plates can serve as local approximations of real-world structures, such as wind turbine blades or aircraft wings, where gradients in refractive index could be applied. To the best of the authors' knowledge, there has been no exploration of GRIN Lens solutions using UD composite materials with a gradient of fiber mass ratio. The present work focuses on the design of a lens for focusing elastic bending waves in a composite plate of constant thickness.

The article is organized as follows. The general design of a gradient-index lens, different gradient-index strategies and the proof of concept design based on the variation of the fiber mass ratio UD composite is are presented in Section 2. The manufacturing process for a composite with a given fiber content between 20% and 62% is selected in Section 3. The performance with a numerical model in terms of energy focusing of the lens designed is shown in Section 4. The lens manufacture and correlation of tests with numerical modeling are presented in Section 5. Finally, the potential applications of the results are discussed in Section 6.

2. Design of a lens for focusing energy

The gradient index lens is integrated into an host plate, as illustrated in (Fig. 1). Bending plane waves are generated at one end of the plate by a series of piezoelectric elements. These A0 mode waves propagate along the x-axis before encountering the lens, which features a gradient of mechanical properties, enabling the waves to be focused in a zone determined by the focusing distance f_l. We indicate the host plate properties with a subscript 0 (.e.g ρ_0 for the density of the host plate) and the lens properties, which are y-dependent, without a subscript (.e.g $\rho(y)$ for the density in the lens).

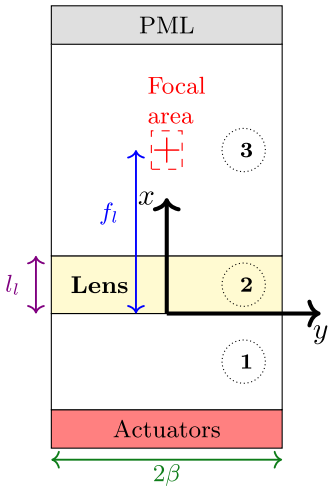

Fig. 1. Top view of GRIN-Lens (zone ②: material properties y gradient) in a host plate (zones ① and ③).

The refractive index represents the ratio of the phase velocities between two media with different properties. Eq. (1) illustrates a secant hyperbolic variation in refractive index, well-known [24,42] for focusing in an isotropic medium:

$$n(y) = \frac{c_0}{c(y)} = n_0 sech(\alpha y) = \frac{n_0}{cosh(\alpha y)} \tag{1}$$

With $\alpha = \frac{\pi}{2f_l}$ (f_l, focal length in m), c_0 and n_0 respectively the phase velocity in m s^{-1} and the refractive index of the host plate ($n_0 = 1$) as shown in Fig. 1, $y \in [-\beta;\beta]$, β half plate width in m.

Under the assumption of unidirectional bending wave propagation along the x-axis, the dispersion equation in isotropic plates [43] is given by Eq. (2).

$$D_x k_x^4 - \rho h \omega^2 = 0 \tag{2}$$

With $D_x = \frac{E_x h^3}{12(1-\nu^2)}$ and k_x wavenumber according x-axis; We deduce from dispersion equation Eq. (2) the phase velocity c, along x-axis Eq. (3).

$$c = \frac{\omega}{k_x} = \sqrt[4]{\frac{D_x \omega^2}{\rho h}} \tag{3}$$

Considering phase velocity equation Eq. (3) under the assumption that the influence of variation of Poisson's ratio is negligible, the refractive index equation Eq. (1) becomes Eq. (4).

$$\frac{E_x(y)h(y)^2}{\rho(y)} = \frac{E_{x_0}h_0^2}{\rho_0}\frac{cosh^4(\alpha y)}{n_0^4} \tag{4}$$

With $E_x(y)$, $\rho(y)$ and $h(y)$ respectively the elasticity modulus along $\vec{x}$ [N m$^-$2], the density [kg m^{-3}] and the thickness [m] of the lens (Fig. 1 zone ②), E_{x0}, ρ_0 and h_0 the elasticity modulus along $\vec{x}$, the density and the thickness of the host plate (Fig. 1 zones ① et ③). Eq. (4) reflects the required space evolution of the properties of the plate to obtain the focusing.

2.1. Various designs

An assumption of Eq. (4) is the isotropy of the domain; however, composite materials are not isotropic. The idea is to use this equation as an initialization point for a GRIN-Lens composite design optimization. Nevertheless, Eq. (4) shows that stiffness, density, and thickness are the design parameters used to define the gradient of a GRIN-lens structure. Consequently, several design strategies can be employed to satisfy Eq. (4). One approach is to use a material with uniform stiffness and density (iso-stiffness and iso-density) while introducing a thickness gradient [10,12–15]. This solution is effective and straightforward to implement but may be restrictive for certain specifications, such as the aerodynamic requirements of an aircraft wing or a wind turbine blade, as mentioned earlier. Alternatively, to meet specific constraints, it is possible to maintain a constant thickness (iso-thickness) while modifying the stiffness and density of the material. Composite materials allow local modification of stiffness. The fiber orientation in a laminate can be adjusted to achieve specific stiffness properties without altering the density. Additionally, both density and thickness can be modified by changing the quantity or type of fibers.

2.2. Fiber mass ratio design

As a proof of concept, UD composites with fibers oriented along the propagation direction (x-axis in Fig. 1) and a variable fiber mass ratio are used to achieve the desired gradient. In this case of a unidirectional composite, applying the mixing laws [44] see Appendix A, Eq. (5) is obtained from Eq. (4).

$$M_f(y) = M_{f0}\frac{cosh^4(\alpha y)}{n_0^4} + \frac{1}{\frac{\rho_m E_f}{\rho_f E_m} - 1}\left(\frac{cosh^4(\alpha y) - 1}{n_0^4}\right) \tag{5}$$

with $M_f(y)$ the fiber mass ratio [%], $M_{f0} = M_f(0)$, ρ_f, ρ_m, E_f and E_m respectively density [kg m^{-3}] and elasticity modulus [N m^{-2}] of fiber and matrix. However, with carbon-epoxy UD [44], $\rho_m E_f \gg \rho_f E_m$ means that the second term of Eq. (5) is negligible see Appendix B for details, Eq. (6) is thus obtained.

$$M_f(y) = M_{f0}\frac{cosh^4(\alpha y)}{n_0^4} \tag{6}$$

The gradient index lens integrated into a UD composite plate is illustrated in (Fig. 1). The variation of the fiber mass ratio along y axis in the lens area according to Eq. (6) is shown by Fig. 2 in solid blue line with $n_0 = 1$, $M_{f0} = 20\%$ and $\alpha = \frac{\pi}{2fl}$ with $f_l = 0.3$ m. Therefore, we have an analytical GRIN-Lens design equation Eq. (6), controlling a single parameter: the fiber mass ratio. The next section describes the manufacturing process proposed to control the fiber mass ratio according to Eq. (6) Fig. 2.

3. Selection of the manufacturing process

The design of a GRIN lens, as described by Eq. (6) exhibits a continuous variation in fiber mass ratio (Fig. 2). From a manufacturing perspective, it is challenging to find a process that can directly achieve this result. However, a discretized lens profile featuring an appropriate number of sectors provides results comparable to a continuous profile [13]. Consequently, the manufacturing strategy involves discretizing the width (2β) of the lens into n sectors, each with a fiber mass ratio Mf_i that matches the dotted red curve shown in Fig. 2. Traditionally, in the use of high-performance composite materials, the objective is to maximize fiber mass ratio. However, the challenge lies in tailoring the fiber mass ratio of a unidirectional composite across a wide range (20% – 62%). In this section, we will explore various composite manufacturing processes and evaluate their efficiency at controlling the fiber mass ratio between 20% and 62%. Given the difficulties associated with composites having a low fiber mass ratio, this section will examine the different processes available to manufacture a (400 × 400 × 3) mm^3 UD carbon/epoxy composite plate with a fiber mass ratio of 20%. Results will be analyzed in terms of fiber mass ratio and thickness relative to target values.

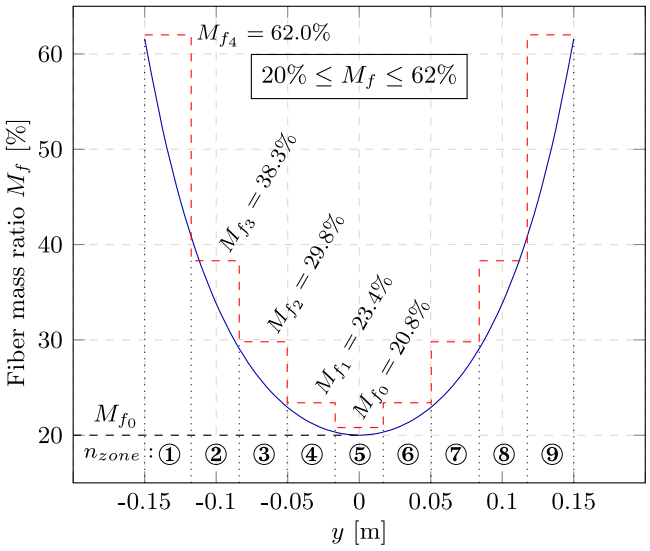

Fig. 2. Fiber mass ratio gradient for a UD carbon-epoxy composite plate, according to Eq. (6) with $M_{f0} = 20\%$, $f_l = 0.3$ m and $n_0 = 1$ (blue continuous line) and discretized gradient in n = 9 sectors (red dashed line).

3.1. Compression molding (CM)

This manufacturing process consists of depositing plies of dry UD carbon fabric in a (400 × 400 × 3) mm^3 mold. Then contact-molding with epoxy resin and placing the mold under pressure. To guarantee a defined fiber mass ratio in a UD carbon/epoxy composite plate, it is necessary to define the number of plies of UD carbon fabric closest to the target fiber mass ratio. Using low grammages of UD fabrics (in this case, 160 g/m^2) is suitable to achieve the desired fiber mass ratio as closely as possible. The values for the mass ratio of fibers that can be manufactured are therefore limited here by the weight of the UD carbon fiber fabric used. This is an important criterion when comparing manufacturing processes. The results of the thickness and fiber mass ratio measurements shown in Fig. 3 demonstrate the difficulty of achieving a target thickness and mass ratio with the implemented process. Moreover, with this process, it is not possible to guarantee a good distribution of fibers in the thickness, as well as in-plane $(\vec{x}, \vec{y})$, fibers are not accurately aligned with x axis. In addition, this process does not provide good impregnation, as it generates void inclusions within the composite. All these defects impact the mechanical properties of the plate, which affects the propagation of bending waves.

3.2. Light RTM (LRTM)

Another manufacturing strategy is to produce the plate using the Light RTM process. This involves placing plies of dry UD carbon fabric in the mold and filling the mold with resin by applying a vacuum (in this case between −0.5 and −0.9 bar). By placing the right number of plies of carbon fabric in the mold, this process achieves a fiber ratio close to 20% by weight. The number of fiber mass ratios that can be produced is limited by the weight of the carbon fabric used. Impregnation is better in this case. However, one of the major problems observed is the displacement of fibers during resin flow. To obtain a low fiber mass, the number of fabric plies is limited. In our case, only six plies are needed in the 3 mm thick mold. As the resin flows, the fibers

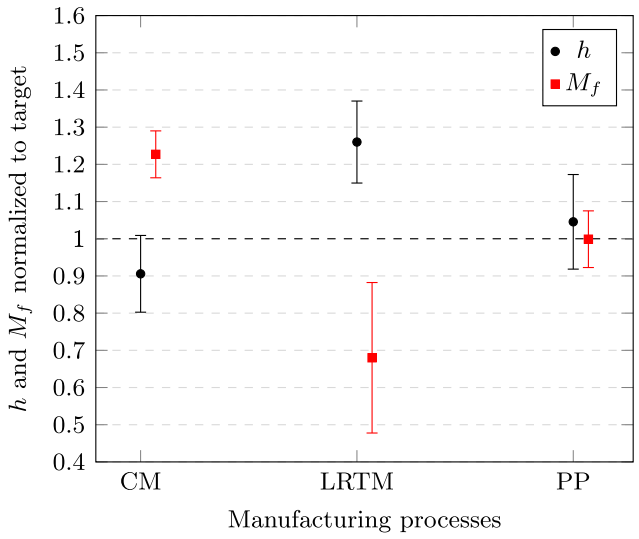

Fig. 3. Mean value and variability ($\pm 2\sigma$) of thicknesses h measured by micrometer *(Testwell® JD300-25)* and fiber mass rates M_f measured by loss on ignition [45, NF EN ISO 10352] obtained with 16 uniformly distributed thickness and fiber mass rate measurements, for each manufacturing process (CM: wet process under press, LRTM: Light RTM, PP: prepregs).

are carried away, resulting in a heterogeneous fiber distribution in the plane plate $(\vec{x}, \vec{y})$ Fig. 4. Variations in thickness and fiber mass ratio were measured on the resulting plate. These measurements are shown in Fig. 3. We observed significant variability in the fiber mass ratio. This manufacturing method could be improved by using a preform obtained from UD plies with a thermoplastic binder.

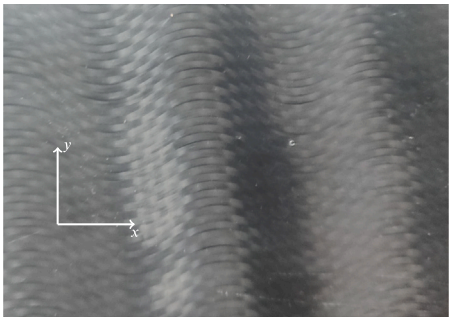

Fig. 4. Fibers displacement resulting from resin flow along the x axis in the LRTM process.

3.3. Prepreg lay-up (pre-impregnated fiber) (PP)

A prepreg is a semi-finished product consisting of a fibrous reinforcement with a thermosetting resin, often epoxy, deposited with precise control over the fiber mass ratio. This process is known for its limited resin flow, which is beneficial in ensuring uniform distribution of fibers throughout the thickness. In order to control the fiber content, the strategy consists of regularly interleaving epoxy adhesive films (here reference Hexbond® ST1035 300g/m^2) during the stacking of prepreg plies (here reference Hexply® M35-4/38%/UD150/37-800). To manage the fiber mass ratio between 20% and the fiber mass ratio of the prepreg 62%, epoxy films are available in very low grammage (75 g/m^2) to achieve the desired thickness and mass ratio. Another significant advantage of this process is that the lens structure can be produced in a single molding, which is not possible with the other two methods, which require several moldings and assemblies to produce the complete lens structure Fig. 1. With this method, we obtain an even distribution of fibers throughout the thickness shown in Fig. 5. Moreover, the fiber thickness and mass ratio values obtained from 16 measurements uniformly distributed over a plate are very close to the target values with low variability $2\sigma = 0.076$ and $2\sigma = 0.127$ respectively for normalized mass ratio and thickness (Fig. 3). Due to these processing advantages and the control of thickness and fiber mass ratio, this process is the most suitable for manufacturing a discretized mass ratio profile. The manufacturing of a prototype is therefore achievable and will be detailed in Section 5.1. But it is necessary to specify the focusing performance of such a design using numerical modeling in Section 4.

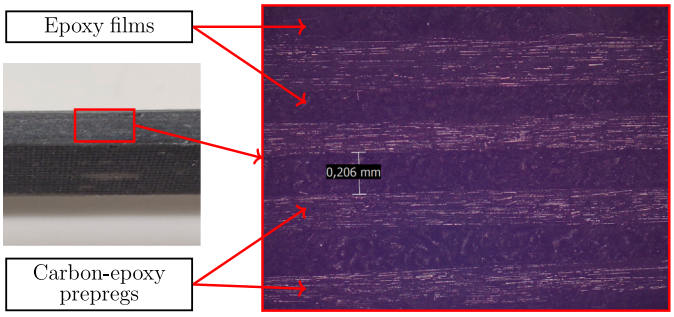

Fig. 5. Position of fibers throughout the thickness in the prepreg process (PP) for a target fiber mass ratio of 20%; sectional view along the fiber direction, obtained using a microscope (Leica DM2700 M).

4. Focusing performance in frequency domain

An analytical equation for designing a UD composite lens with the fiber mass ratio (Eq. (6)) as the design variable was introduced in Section 2. In Section 3, we demonstrated the ability to manufacture a UD composite structure with a specific fiber mass ratio. The dimensions of the plate and therefore the frequency range are constrained by the experimental measurement. This dimensioning is detailed below in Section 4.1 and in Section 5.1 for manufacturing. The objective of this section is to begin from the operating point, assuming isotropy as per Eq. (6), to determine whether the focusing phenomenon occurs within a specified frequency range and to delineate its performance.

4.1. Numerical model

A numerical simulation of the UD composite GRIN Lens was conducted using the commercial software COMSOL Multiphysics® [46].

The prepreg lay-up manufacturing process seclected in Section 3 enables extreme variation in fiber mass ratio M_f ranging from 20% to 62%. To exploit this manufacturable range, the design equation (Eq. (6)) for $y = \pm\beta$ sets $M_{f0} = 20\%$ and $M_f(\pm\beta) = 62\%$. As initialization point, a focal length of $f_l = l_l = 300$ mm was chosen, resulting in $2\beta = 300$ mm lens width. The numerical calculation of the GRIN composite lens shows a much longer focal length. This discrepancy was attributed to material anisotropy. An optimization loop with geometric parameters of the lens highlight that with a much longer lens length $l_l = 600$ mm, the composite GRIN-Lens focus at $f_l = 700$ mm. Fig. 6 represents the geometry of the GRIN-Lens with $2\beta = 300$ mm width and $l_l = 600$ mm length, other dimensions of the plate are $l_1 = 330$ mm, $l_2 = 800$ mm corresponding respectively to the host plate before and after the lens area. These dimensions take into account experimental measurement constraints. To observe a plane wavefront and verify the wavelength λ before the lens, a minimum of 2λ is required for l_1. According to Eq. (7) and Table 2, for 2000 Hz waves, the wavelength is 129.4 mm, satisfying the condition $l_1 > 2\lambda$. Therefore, 2000 Hz will be the lower bound of the frequency range for the manufactured prototype lens. To prevent reflections and ensure clear observation of the focusing phenomenon, a Perfectly Matched Layer (PML) [47] is implemented as a perfect absorption zone. PML zones, each measuring $l_{pml} = 200$ mm in length, are positioned one before the excitation line

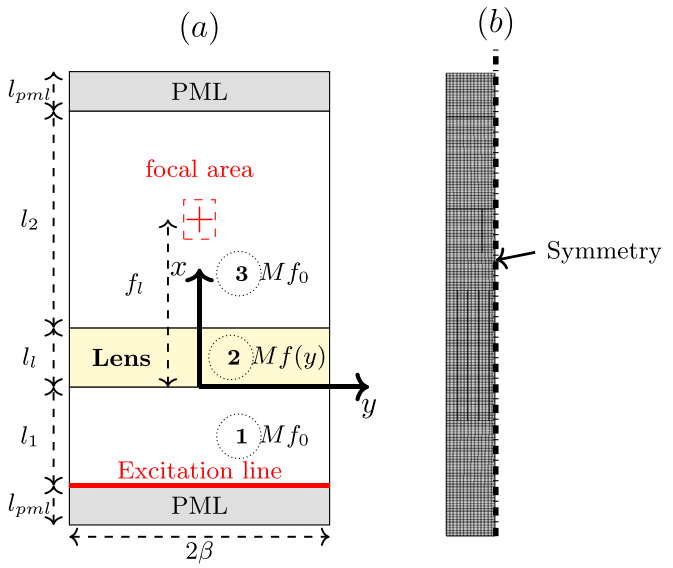

Fig. 6. (*a*) Geometry of the GRIN-Lens Numerical Model; (*b*) Mesh for frequency $f = 2000$ Hz.

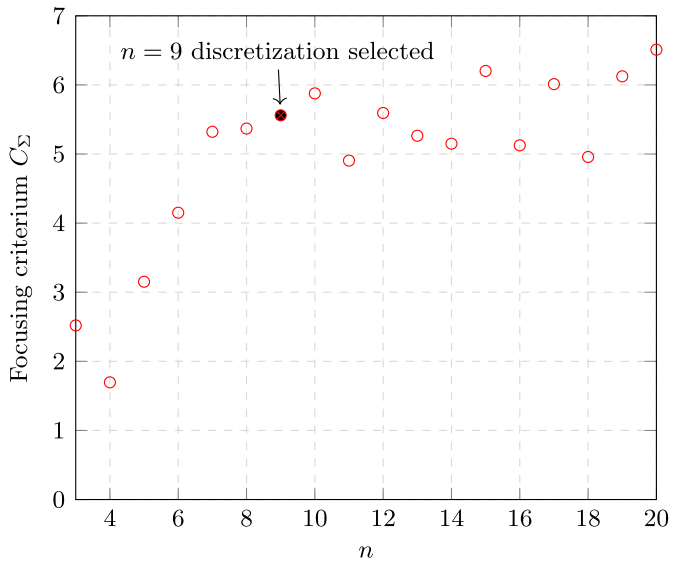

Fig. 7. Effect of gradient discretization on the focusing performance for $f = 8000$ Hz; Performance criterion C_ϵ described in Section 4.2.

and another at the opposite end past the lens to minimize reflections. As PML elements are not supported for 2D plate elements in COMSOL Multiphysics® [46], a high damping ratio was utilized for the PML zones instead. A harmonic out-of-plane loading force along the z-axis at a frequency f is applied to the excitation line (indicated by the red line in Fig. 6). The mesh is composed of rectangular second-order elements and the element length is chosen to ensure 10 finite elements per wavelength. This means that before the computation is executed, the wavelength Eq. (7) is computed as a function of the frequency and the properties of the host plate from dispersion equation Eq. (2). The study was limited to a frequency of 8 kHz. Increasing the frequency leads to incrementally longer computation and measurement times due to the prototype's dimensions. However, this frequency is not a fundamental operating limit of the lens.

A continuous profile of fiber mass ratio is difficult to manufacture we choose to discretize GRIN-Lens width (2β) in $n = 9$ sectors, that is 33 mm width. Fig. 7 illustrated the effect of gradient discretization on focusing performance evaluated for $f = 8000$ Hz using performance criterion C_ϵ described in Section 4.2. A discretization level of $n = 9$ is selected, as it provides the optimal balance between focusing performance, manufacturing complexity and time.

The dedicated fiber mass ratio selected for each sector is as close as possible to the maximum of the continuous fiber mass ratio on the sector Fig. 2. GRIN Lens profile is symmetrical and the fiber mass ratio value from the central sector to the extremum sector are $Mf_0 = 20.8\%$, $Mf_1 = 23.4\%$, $Mf_2 = 29.8\%$, $Mf_3 = 38.3\%$ and $Mf_4 = 62,0\%$. To implement materials properties of each sector of the lens and the host plate we homogenized UD carbon-epoxy composite material with his dedicated fiber mass ratio using mixing law [44]. Variations in material properties (i.e. density ρ, elasticity moduli E_x, E_y, G and Poisson's coefficients ν_{xy}, ν_{yz}) are presented in Fig. 8 as a function of fiber mass ratio using mixing law with the properties of carbon fiber and epoxy resin in Table 1 and equations are detailed in Appendix A.

$$\lambda = \frac{c}{f} = \frac{2\pi}{k_x} = 2\pi\sqrt[4]{\frac{D_x}{\omega^2 \rho h}} \tag{7}$$

4.2. Performance criteria

The GRIN-Lens system enables the focussing of waves, specifically progressive mechanical flexural waves, as investigated in this study.

Table 1
Mechanical properties of fiber and matrix, featuring (1) longitudinal axis and (2) transverse axis of fibers.

Parameter	Property	[Unit]	Value
Fiber			
ρ_f	Density	[kg m^{-3}]	1820
E_{1_f}	Elastic modulus 1	[GPa]	278
E_{2_f}	Elastic modulus 2	[GPa]	40
G_{12_f}	Shear modulus	[GPa]	15
ν_{12_f}	Poisson's ratio		0.2
Matrix			
ρ_m	Density	[kg m^{-3}]	1280
E_m	Elastic modulus	[GPa]	3
ν_m	Poisson's ratio		0.4

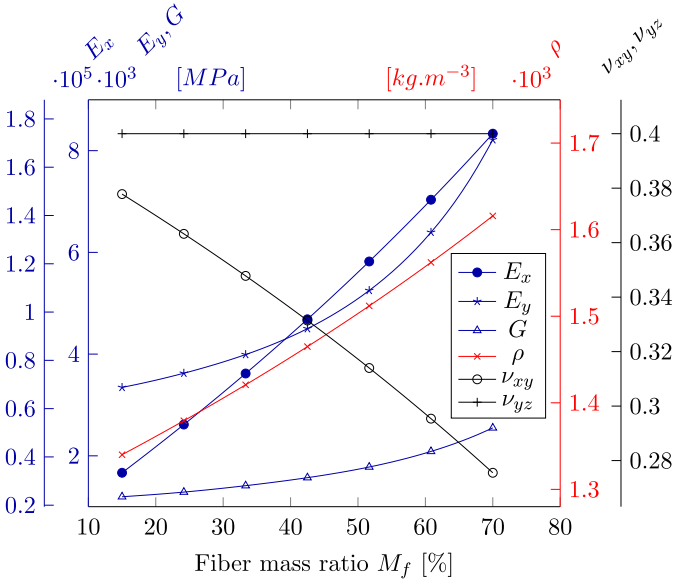

Fig. 8. Material properties of UD composite as a function of fiber mass ratio M_f, using the mixing law homogenization method [44]; with axis $\vec{x}$ indicating the direction of fibers.

A progressive mechanical flexural wave propagates through a material medium, causing a local displacement of elementary particles in a direction orthogonal (z-axis) to the wave's propagation direction (x-axis), thereby transporting energy. Focusing refers to the act of concentrating energy on a point or within an area. Indeed, a way to measure the focalization of progressive mechanical flexural waves in an area is to compare the density of energy in this focal area (Fig. 1) with the density of energy of a structure with no focus and therefore no lens. Because a progressive mechanical flexural wave causes a local displacement of elementary particles in the material medium in the direction orthogonal (z-axis), a way to express energy density is the sum of the kinetic energy of particles in the focal area divided by the surface of the focal area Eq. (8).

$$\Sigma_k = \frac{1}{S_f}\left[\frac{1}{2}m\iint_{S_f} v_z(x,y)^2 \mathrm{d}x\mathrm{d}y\right] \tag{8}$$

With S_f the surface of the focal area, $m = \rho_0 S_f h_0$ the total mass of the focal area with ρ_0, h_0 respectively the host plate density and thickness and $v_z(x,y)$ the z-axis velocity of element at (x,y) position. To compare results for different frequencies, the focal area is defined by a width (y-axis) of 0.5λ and a length (x-axis) of 2λ, so the focusing area S_f is λ^2. Therefore, the kinetic energy density criterion is the ratio of kinetic energy density in the focal zone for a plate with a GRIN-Lens with a plate without GRIN-Lens Eq. (9). Mass m and integration surface S_f are identical in both configurations, consequently, they vanish from the evaluation criterion.

$$C_\Sigma = \frac{\Sigma_{k_l}}{\Sigma_{k_0}} = \frac{\iint_{S_f} v_{z_l}(x,y)^2 \mathrm{d}x\mathrm{d}y}{\iint_{S_f} v_{z_0}(x,y)^2 \mathrm{d}x\mathrm{d}y} \tag{9}$$

With Σ_{k_l} and Σ_{k_0} respectively the kinetic energy density of the plate with a GRIN-Lens and the plate without GRIN Lens. This criterion C_Σ represents the energy density gain in the defined focal area provided by the GRIN-Lens.

Another way used to determine the focusing performance of a GRIN-Lens system is the FWHM (Full Width at Half Maximum) used like in [48]. The principle is to compare the width of the focal spot (y-axis) to the wavelength. We need to evaluate values of out-of-plane velocity (z-axis) along the y-axis at the x-coordinate of the maximum velocity Fig. 9. The smaller the FWHM value in front of the wavelength, the better the focusing performance.

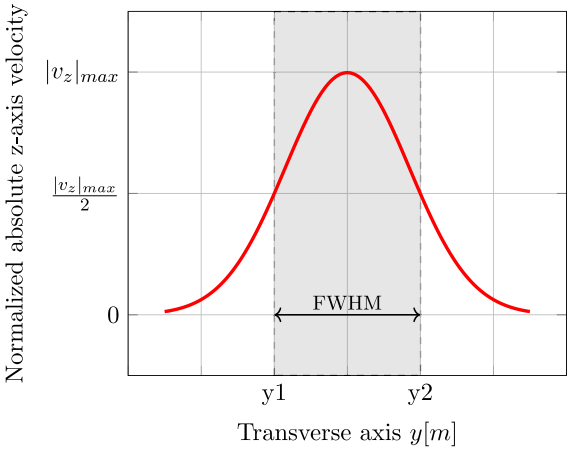

Fig. 9. Full width at half maximum criterium principle.

4.3. Numerical results

Some harmonic responses for an excitation frequency f between 2 kHz to 8 kHz are obtained. In Fig. 10 we observed the normalized absolute out-of-plane velocity field for 4 frequencies, respectively 2000 Hz, 4400 Hz, 5800 Hz and 8000 Hz. A focusing effect is observed with focal spot size proportional to the wavelength Eq. (7) corresponding to the excitation frequency f. To specify the focusing performance of this design GRIN-Lens we compute the energy density gain C_Σ and FWHM criteria for these excitation frequencies like in Fig. 11 for $f = 8000$ Hz. Table 2 gives these criteria results. The energy density gain C_Σ criterion is variable with frequency, being around 3 for $f = 2000$ Hz and $f = 5800$ Hz, and 5 for $f = 4400$ Hz and $f = 8000$ Hz. This discrepancy can be explained by side-effects see Fig. 10, but these results highlight that the GRIN-Lens system increases the energy density in the focusing zone by a factor of 3 to 5. FWHM values are consistent, FWHM$\approx 0.4\lambda$, lower than λ, indeed subwavelength focusing is numerically observed for excitation frequencies between 2 kHz to 8 kHz, for the fiber mass ratio composite GRIN-Lens design Fig. 2. These numerical results are promising for manufacturing to provide experimental proof of this GRIN-Lens design.

Table 2
Focusing criteria results.

Frequency [Hz]	λ [mm]	FWHM	C_Σ
2000	129.4	0.41	2.52
4400	86.5	0.39	4.99
5800	75.3	0.41	3.23
8000	63.6	0.39	5.56

5. Manufacturing and experiments

5.1. Manufacturing

The manufacturing process selected in Section 3 is the prepreg lay-up; the benefits and advantages of this process for GRIN-Lens manufacturing are outlined. The principle of this process relies on interleaving of prepreg (Hexply® M35-4/38%/UD150/37-800) and epoxy film (Hexbond® ST1035 300 g/m^2). The ratio of prepreg plies to epoxy film plies manages the fiber mass ratio. For instance, to achieve a fiber mass ratio of $M_{f_0} = 20.8\%$ in the host plate, it requires 5 prepreg plies and 8 epoxy film plies, a proportion of 38.5% of prepreg plies. The GRIN-Lens fiber mass ratio profile is symmetrical and has been discretized into 9 sectors; the proportions of prepreg plies for all these sectors are listed in Table 3. This process necessitates a lot of plies cutting, the entire lens structure with the host plate represents around 200 layers. These cuts were initially made by hand but can also be performed using a numerically-controlled machine to reduce time and improve repeatability. Furthermore, the hand-layup in the open mold is time-consuming as it requires placing the mold under vacuum approximately every two layers during lay-up to prevent air from being trapped in the structure. The total manufacturing time, including curing (30 min @ 150 °C) is approximately 14 h. To generate planar flexural waves, 7 low-cost disk-shaped PZT patches ($diameter = 25$ mm, $thickness = 135$ µm) are uniformly bonded along the excitation line, as illustrated in Fig. 1. The detailed properties of these PZT patches can be found in [49]. At the top edge, viscoelastic layers are added to simulate PML effects, absorb incoming waves and minimized reflections. The layers consist of a 5 mm thick 3M VHB polymer on both sides of the plate, secured by a 1 mm thick aluminum plate. Numerical calculation shows that a PML zone length greater than 2λ ensures low reflections as well as performed in [13]. According to the frequency range, the length of this PML area is set to 300 mm, which is selected to guarantee a minimum length of 2λ for incident 2000 Hz waves with $\lambda = 129.4$ mm see Table 2. For experimental measurement, the plate is suspended by the aluminum plates and coated with white paint to ensure good reflection for the laser vibrometer.

5.2. Wave propagation measurement

Experimental measures are made with a scanning laser Doppler vibrometer *(Polytec PSV-500-H)* Fig. 12. A burst-type reference signal of 0.5 V amplitude, 0.5 ms duration and 8000 Hz center frequency is amplified (×20) and applied to the 7 piezoelectric elements connected

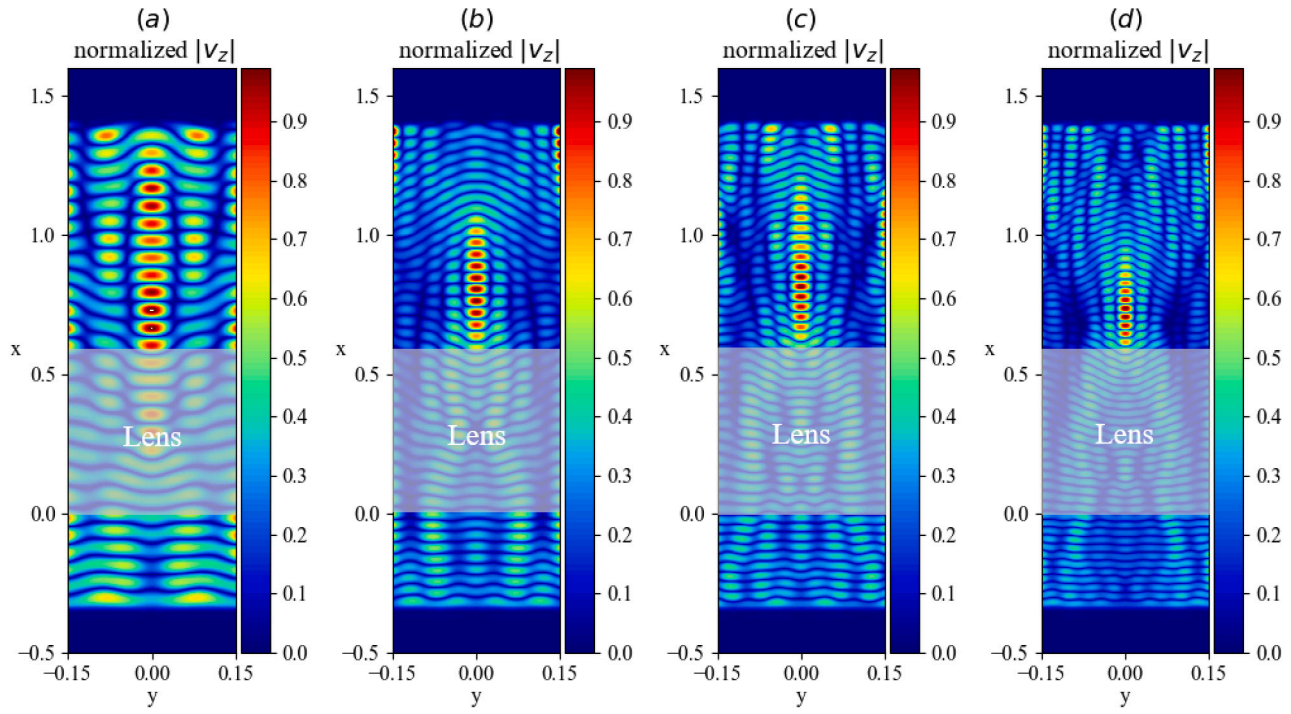

Fig. 10. Normalized absolute out-of-plane velocity field for a harmonic computation at a frequency of (a) 2000 Hz; (b) 4400 Hz; (c) 5800 Hz and (d) 8000 Hz.

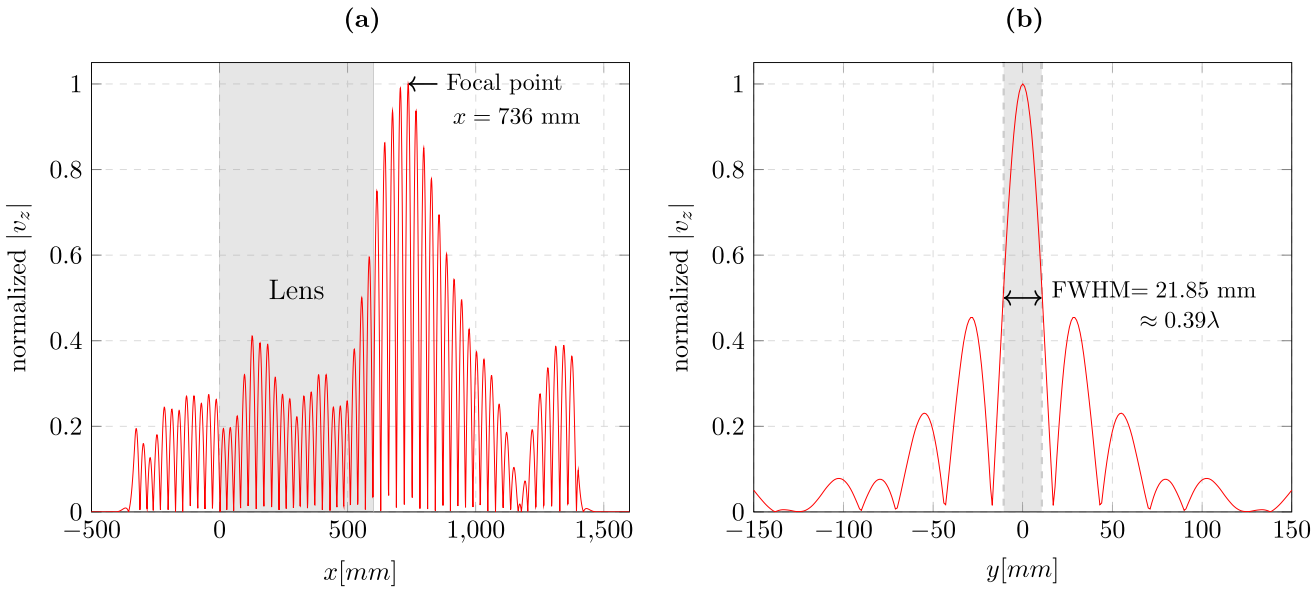

Fig. 11. (*a*) Normalized absolute out-of-plane velocity $|v_z|$ along x-axis for $f = 8000$ Hz; (*b*) Full Width at Half Maximum criterium for $f = 8000$ Hz at $x = 736$ mm.

Table 3
Percentage of lens composite prepreg plies and corresponding theoretical fiber mass ratio Mf; HP (host plate, i.e., zones ① and ③ as shown in Fig. 1); carbon-epoxy prepreg (Hexply® M35-4/38%/UD150/37-800) and epoxy film (Hexbond® ST1035 300 g/m²); Prepreg UD plies are oriented in $\vec{x}$ direction (see Fig. 1).
,abovefloat=5pt

Proportions	n_{zone}				
	1;9	2;8	3;7	4;6	5;HP
Prepreg [%]	100	66.6	53.3	42.8	38.5
Mf [%]	62.0	38.3	29.8	23.4	20.8

in parallel, in order to generate a plane wave packet that will propagate in the plate. From this reference signal, laser vibrometer measures the out-of-plane displacement for 3 ms at a sampling frequency of 80 kHz for all points of a regular squared mesh of (130 × 25) points. Then from the displacement field, the velocity field is computed and the normalized absolute out-of-plane wave field velocity at focusing time (t = 1.788 ms) is shown by Fig. 14(a),(d) and the animation of the propagation is in the supplementary data. This measurement is an experimental proof of the validity of the GRIN-Lens design approach based on fiber mass ratio profile of a UD composite. We observed a focalization at $x \approx 800$ mm like in the harmonic responses Fig. 10d. To be able to compare numerical simulation to measurements, it is necessary to get the numerical computation of the time response of a burst excitation signal as in the experiment.

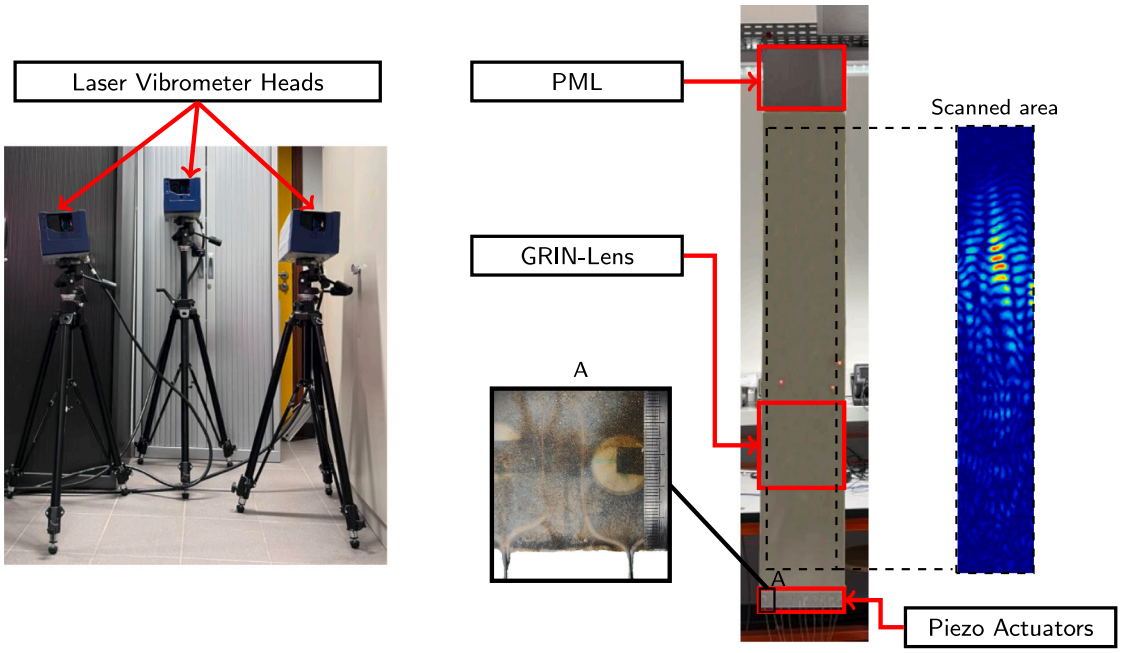

Fig. 12. Experimental setup.

5.3. Experimental–numerical correlation

For the Experimental-Numerical correlation, a transient numerical simulation is done using the commercial software COMSOL Multiphysics® [46]. To make the excitation equivalent to the experiments, the excitation line Fig. 6a is discretized into 7 segments corresponding to the diameters of the piezo patches and a burst type equivalent load with a duration of 0.5 ms and 8000 Hz center frequency is applied to these segments. The amplitude is set to 35N to matched the total kinetic energy before the end of excitation at $t = 0.6$ ms see Fig. 13. Experiment curve Fig. 13 shows that total kinetic energy of the plate decrease due to damping. Therefore, Rayleigh damping [50] with damping values of 0.005 and 0.01 respectively for 2000 Hz and 8000 Hz is set to obtain the correlation of total kinetic energy shown by Fig. 13. Numerical results 14(c),(f) respectively for 2 kHz and 8 kHz are in agreement with experiments 14(a),(d) concerning focusing distance and propagation velocity, based on the normalized absolute out-of-plane wave field velocity. At the moment when the maximum energy is focused at t = 2.806 ms for 2 kHz and t = 1.778 ms for 8 kHz Fig. 14, the focal spot appears in a similar position and shape in both cases, respectively. The focusing performance criteria discussed in Section 4 were used to compare the experimental results with the simulations. The wavelengths obtained for the simulations are 131.0 mm and 63.6 mm, for 2 kHz and 8 kHz respectively, whereas the experimentally measured are 129.4 mm and 71.6 mm respectively as reported in Table 4. This discrepancy can be attributed to material properties uncertainties (such as stiffness E_x, thickness h and density ρ) as indicated by the wavelength equation Eq. (7). For the FWHM criteria Table 4, values from simulations and experiments are close, with 0.41λ (simulation) and 0.37λ (experiment) at 2 kHz and 0.47λ (simulation) and 0.58λ (experiment) at 8 kHz Fig. 15. In contrast, minor discrepancies in the location and amplitude of secondary peaks may result from material properties variation or assembly-induced residual stresses. We observed on experiments at the beginning of the animation see in supplementary data that one of the seven piezoelectric patch was non-functional, contributing to the asymmetry of the out-of-plane velocity profile along y-axis at the focal spot Fig. 15. The energy density criterion C_Σ Eq. (9) for simulations are obtained with numerical results with GRIN-Lens structure Fig. 14(a),(c) and without GRIN-Lens structure Fig. 14(b),(e), for experimental computation of the criterion the numerical results without GRIN-Lens structure are used instead of a manufactured carbon-epoxy plate, for material savings. For the numerical results without lens Fig. 14(b),(e), waves are not strictly planar due to the excitation generated by the seven piezoelectric transducers and the influence of side boundary effects, ensuring correlation with the experimental setup Fig. 11. According to this criterion, the energy density gain of the GRIN-Lens structure at focus time in the focal area ($0.5\lambda \times 2\lambda$) is respectively 3.25 and 2.61 for simulation and experiment for 2 kHz and 7.65 and 7.32 for simulation and experiment for 8 kHz Table 4. The lower energy density gain C_Σ for 2 kHz is due to edge effects and reflections in the simulation without the lens Fig. 14(b), which increase the kinetic energy density in the focus zone for the plate without lens, Σ_{k_0} in Eq. (9). Focusing effect of the manufactured composite GRIN-Lens is observed and evaluated by the focusing criteria, which are in good agreement between simulation and experiment for the limits 2 kHz and 8 kHz of the studied frequency range.

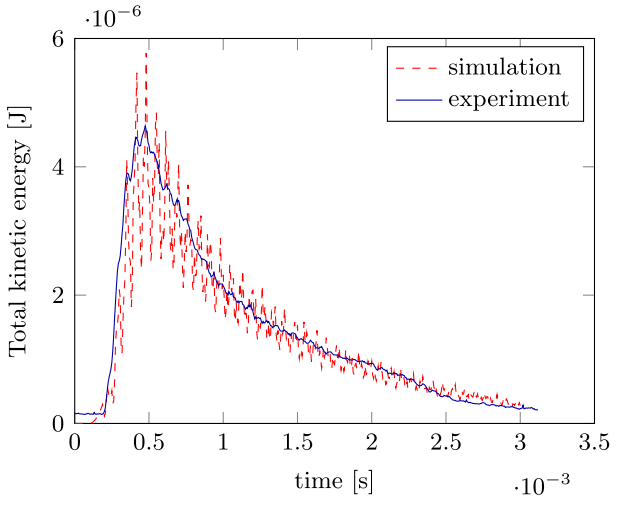

Fig. 13. Evolution of total plate kinetic energy for 8 kHz input waves numerical and experimental results.

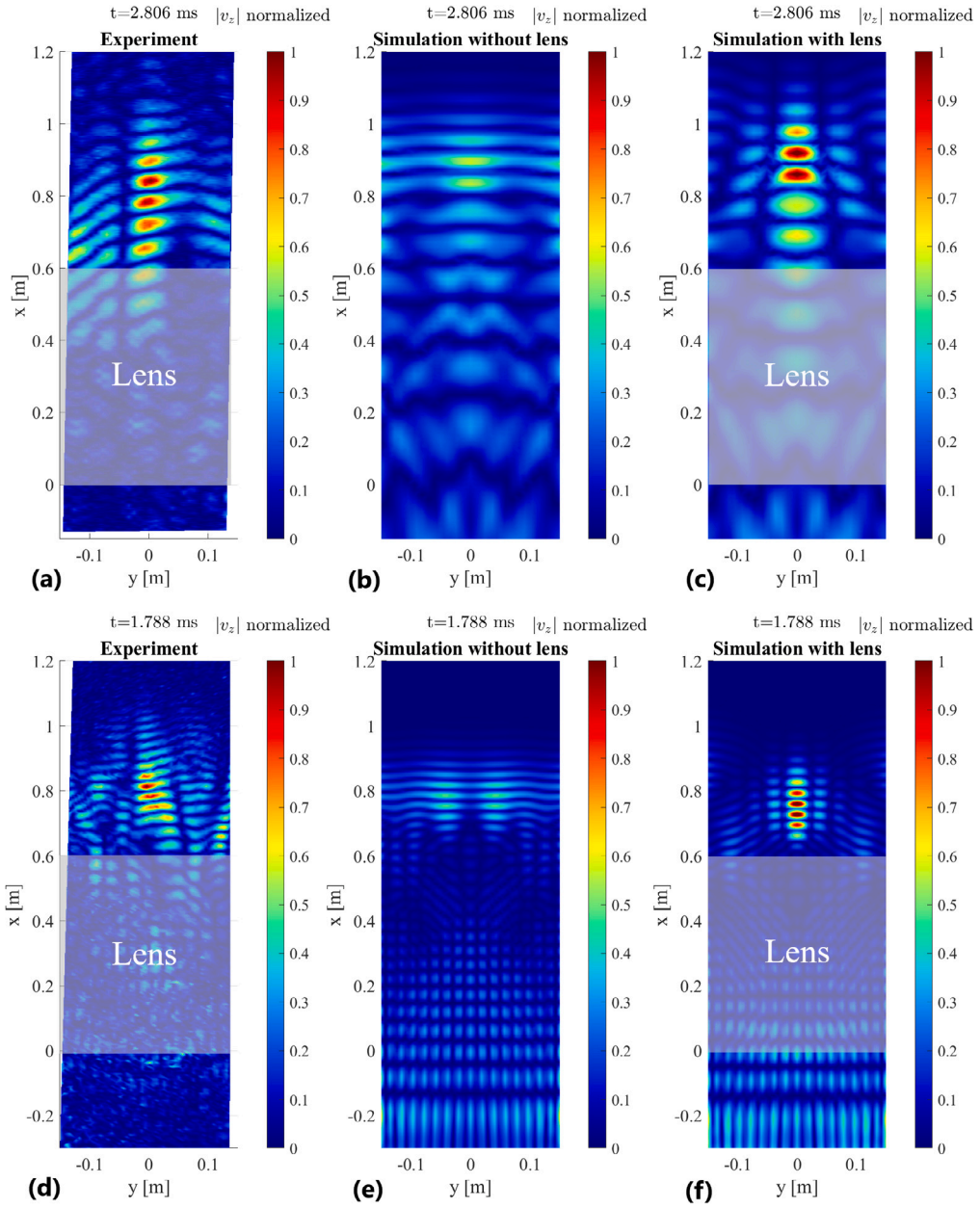

Fig. 14. Comparison of normalized absolute out-of-plane wave field velocity for an incident plane flexural wave at focusing time for two frequencies: 2000 Hz and 8000 Hz. For 2000 Hz, (a) experimental result of the manufactured plate with a composite lens structure, measured using a scanning laser Doppler vibrometer *(Polytec PSV-500-H)*; (b) shows numerical result of a plate without lens and (c) shows numerical result of a plate with lens. For 8000 Hz, (d), (e), and (f) present the same comparisons, respectively; **See supplementary data for the wave propagation video**.

Table 4
Comparison of focusing criteria between simulation and experiment at focusing time for $f = 2$ kHz and $f = 8$ kHz.

Frequency	λ (mm)	FWHM	S_f (mm^2)	C_Σ
2 kHz				
Simulation	129.4	0.41	16744.4	3.25
Experiment	131.0	0.37	17161.0	2.61
8 kHz				
Simulation	63.6	0.47	4045.0	7.65
Experiment	71.6	0.58	5126.6	7.32

6. Applications

Efficient energy management is a key challenge in the development of smart structures [6], where the ability to harvest and utilize energy effectively is crucial for powering embedded systems and enabling data transmission at higher frequency and over longer distances. The GRIN-lens design presented in this study offers a promising solution, it is capable of increasing energy density by a factor of 7 in the ($2\lambda \times 0.5\lambda = \lambda^2$) focus zone. This means that an energy harvester located at the focus zone could get up to 7 times more energy than an energy harvester located in the same zone without GRIN-Lens. Performance comparison is complicated due to the dependency of the focusing criterion on the dimensions of the focus zone relative to the wavelength or the harvesting device used. Gradient-index phononic crystals exhibits an amplified harvesting power of 3.8 times [9] or 2.84 times [27], these gains are evaluated with an 8 mm [9] or 7 mm [27] diameter piezoelectric ceramic disc, corresponding to a $0.13\lambda^2$ [9] a $0.78\lambda^2$ [27] surface. Thickness strategy energy harvesting [15] demonstrated a 2.5 energy ratio gain with a 25 mm diameter piezoceramic transducers (PZT). An energy

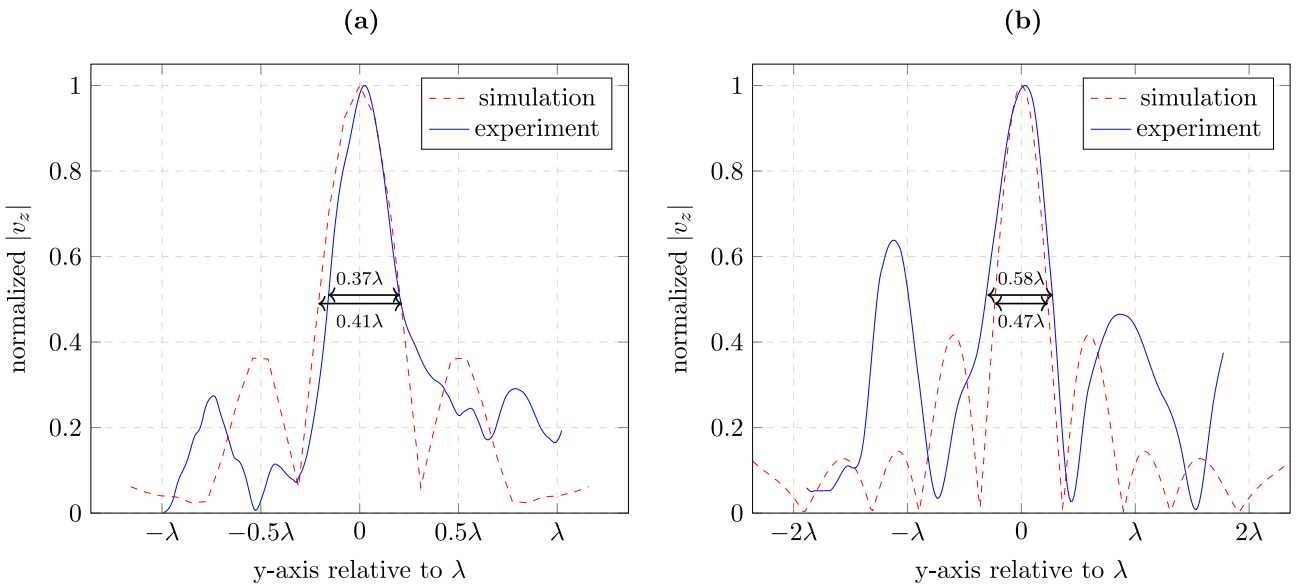

Fig. 15. Comparison between lateral profile of normalized out-of-plane velocity at focus time and focal length for simulation and experiment (a) for $f = 2$ kHz and (b) for $f = 8$ kHz.

ratio of 7 was reached by shunted piezoelectric lattice lens [16] with a dedicated surface evaluation. Considering a large focus zone evaluation (λ^2), fiber mass ratio modulation strategy for the GRIN-Lens design with an energy gain of 7 appears to be a good performance compared to phononic crystals, thickness or shunted piezoelectric lattice strategies. Furthermore, the versatile design strategies provided by composite materials and a wide operating frequency range enable these structures to be better suited to existing specifications, minimizing their intrusive impact. Such an enhancement could significantly contribute to improving the performance and autonomy of smart structures in applications like structural health monitoring and self-powered technologies.

7. Conclusion

This work shows that the design freedoms of composite materials allow a new approach to GRIN lens design in a constant thickness plate. A gradient of density and stiffness can be obtained by adjusting the fiber mass ratio of a composite structure. Various manufacturing processes were compared to determine the most suitable one for controlling the fiber mass ratio of iso-thickness plate. It has been demonstrated that it is possible to focus the energy of an elastic bending wave in a UD composite plate by controlling this fiber mass ratio in a wide frequency range (2–8 kHz). The manufacturing process chosen for best control of the fiber mass ratio is the prepreg process, with carbon prepreg and epoxy plies interleaved. With this process, we are able to control the fiber mass ratio over a range from 20% to 62%, which is consistent with the dimensioning of the fiber mass ratio gradient required to focus considering the properties of carbon fibers and epoxy used. The study presented here was conducted on a non-standard host structure made of unidirectional carbon-epoxy (fiber volume fraction 20%), but the design approach is applicable to other types of host structures. However, depending on the mechanical properties of the host, it may be difficult to find a working configuration for a constant-thickness GRIN lens, particularly if the structure cannot be sufficiently stiffened to achieve the required modulation of flexural wave velocity for focusing. In such cases, it may be necessary to locally increase the stiffness by adding thickness. This additional thickness can remain relatively low when using composite materials, especially considering that for flexural behavior, the outermost layers are the most influential. It is therefore possible to design a GRIN lens based on an existing structure with known properties by applying the methodology presented in this study to determine the required modifications and assess whether they remain within the overall design constraints. The analytical equation dimensioning focusing in a plate highlights a continuous gradient of fiber mass ratio. However, we have shown with a numerical model and then with the manufacture of the plate that the discretization of the gradient does not hinder the focusing of the energy. The discretization of the gradient improves the manufacturing feasibility, it is easier to discretize the gradient in sectors rather than to manufacture a continuous variation of properties. The comparison between the numerical model and the measurements made on the manufactured lens made it possible first of all to take into consideration the damping properties of the materials used. Then we were able to highlight that the energy density in a defined focusing zone can be increased by a factor of 7 with a gradient lens composite structure, for an incident wave of 8 kHz. Furthermore, the experiment yielded a FWHM value of 0.58λ, with manufacturing uncertainties likely accounting for the differences between the simulation and experimental results. The design criteria and analytical dimensioning equations outlined provide a foundation for designing and implementing systems such as energy harvesting devices in composite structures. It is also important to note that successful lens design relies on a good understanding of the actual loading conditions of the part during operation, particularly the wave front shape, the direction of the flexural waves and their frequency range even though the proposed solution exhibits broadband performance. To advance this work, conducting a mechanical characterization of the lens structure would be beneficial to identify manufacturing uncertainties as part of a robust design approach.

CRediT authorship contribution statement

Valentin Rapine: Writing – original draft, Validation, Software, Methodology, Investigation, Formal analysis, Data curation, Conceptualization. **Nour Abuhemeida:** Validation, Software, Methodology, Investigation, Formal analysis, Data curation, Conceptualization. **Morvan Ouisse:** Project administration, Methodology, Funding acquisition, Formal analysis, Data curation, Conceptualization, Writing – review & editing, Validation, Supervision. **Scott Cogan:** Methodology, Funding acquisition, Writing – review & editing, Validation, Supervision, Project administration, Formal analysis, Data curation, Conceptualization. **Pascal Francescato:** Writing – review & editing, Validation, Supervision, Project administration, Methodology, Funding acquisition, Formal analysis, Data curation, Conceptualization. **Rémy Lachat:** Writing – review

& editing, Validation, Supervision, Project administration, Methodology, Funding acquisition, Formal analysis, Data curation, Conceptualization. **Yann Meyer:** Writing – review & editing, Validation, Supervision, Project administration, Methodology, Funding acquisition, Formal analysis, Data curation, Conceptualization.

Declaration of competing interest

The authors declare the following financial interests/personal relationships which may be considered as potential competing interests: Rapine Valentin reports financial support was provided by French National Research Agency. If there are other authors, they declare that they have no known competing financial interests or personal relationships that could have appeared to influence the work reported in this paper.

Acknowledgments

This research was funded, in whole or in part, by l'Agence Nationale de la Recherche (ANR), project ANR-21-CE46-001. For the purpose of open access, the author has applied a CC-BY public copyright licence to any Author Accepted Manuscript (AAM) version arising from this submission.

Appendix A. UD composite mixing laws equations

For a unidirectional (UD) composite consisting of two phases, the fiber volume ratio and the fiber mass ratio are related as shown in Eq. (A.1). The properties of the fiber and matrix are listed in Table 1.

$$V_f = \frac{M_f}{M_f + \frac{\rho_f}{\rho_m}(1 - M_f)} \tag{A.1}$$

Subsequently, the mixing laws [44] define all properties of the UD composite material.

$$\rho = \rho_f V_f + \rho_m (1 - V_f) \tag{A.2}$$

$$E_x = E_{x_f} V_f + E_{x_m} (1 - V_f) \tag{A.3}$$

$$E_y = \frac{1}{\frac{V_f}{E_{y_f}} + \frac{1 - V_f}{E_m}} \tag{A.4}$$

$$G_{xy} = \frac{1}{\frac{V_f}{G_{xy_f}} + \frac{1 - V_f}{G_m}} \tag{A.5}$$

$$\nu_{xy} = \nu_f V_f + \nu_m (1 - V_f) \tag{A.6}$$

Appendix B. Carbon-epoxy fiber mass ratio simplified design equation

From UD composite mixing laws detailed in Appendix A, the ratio of Young's modulus along the x-axis to density $\frac{E_x}{\rho}$ could be written as a function of fiber mass ratio M_f as in the Eq. (B.1).

$$\frac{E_x}{\rho} = A M_f + \frac{E_m}{\rho_m} \tag{B.1}$$

With $A = \dfrac{\rho_m (E_f - E_m) - E_m (\rho_f - \rho_m)}{\rho_f \rho_m}$

Using Eq. (B.1), Eq. (4) is transformed into Eq. (B.2).

$$M_f(y) = M_{f_0} cosh^4(\alpha y) + \frac{E_m}{A \rho_m} \left(cosh^4(\alpha y) - 1 \right) \tag{B.2}$$

With $\dfrac{E_m}{A \rho_m} = \dfrac{1}{\frac{\rho_m E_f}{\rho_f E_m} - 1}$

According to the mechanical properties of carbon-epoxy listed in Table 1, $\frac{E_m}{A \rho_m} = 0.0188 \ll M_{f_0} = 0.2$. Therefore Eq. (B.2) could be reduced to Eq. (5).

Appendix C. Supplementary data

Supplementary material related to this article can be found online at https://doi.org/10.1016/j.compstruct.2025.119500.

Data availability

Data will be made available on request.

References

[1] Wood OJ, Featherston CA, Kennedy D, Eaton MJ, Pullin R. Optimised vibration energy harvesting for aerospace applications. Key Eng Mater 2012;518:246–60. http://dx.doi.org/10.4028/www.scientific.net/KEM.518.246, URL: https://www.scientific.net/KEM.518.246, Publisher: Trans Tech Publications Ltd.

[2] Zelenika S, Hadas Z, Bader S, Becker T, Gljušćić P, Hlinka J, Janak L, Kamenar E, Ksica F, Kyratsi T, Louca L, Mrlik M, Osmanović A, Pakrashi V, Rubes O, Ševeček O, Silva JPB, Tofel P, Trkulja B, Unnthorsson R, Velagić J, Vrcan Z. Energy harvesting technologies for structural health monitoring of airplane components—A review. Sensors 2020-01;20(22):6685. http://dx.doi.org/10.3390/s20226685, URL: https://www.mdpi.com/1424-8220/20/22/6685, Number: 22 Publisher: Multidisciplinary Digital Publishing Institute.

[3] Memmolo V, Monaco E, Boffa ND, Maio L, Ricci F. Guided wave propagation and scattering for structural health monitoring of stiffened composites. Compos Struct 2018-01-15;184:568–80. http://dx.doi.org/10.1016/j.compstruct.2017.09.067, URL: https://www.sciencedirect.com/science/article/pii/S0263822317330520.

[4] Gaudenzi P. Introduction to smart structures. In: Smart structures. John Wiley & Sons, Ltd; 2009, p. 1–34. http://dx.doi.org/10.1002/9780470682401.ch1, URL: https://onlinelibrary.wiley.com/doi/abs/10.1002/9780470682401.ch1.

[5] Meyer Y, Lachat R, Akhras G. A review of manufacturing techniques of smart composite structures with embedded bulk piezoelectric transducers. Smart Mater Struct 2019-04;28(5):053001. http://dx.doi.org/10.1088/1361-665X/ab0fab, Publisher: IOP Publishing.

[6] Lampani L, Gaudenzi P. Innovative composite material component with embedded self-powered wireless sensor device for structural monitoring. Compos Struct 2018-10-15;202:136–41. http://dx.doi.org/10.1016/j.compstruct.2018.01.011, URL: https://www.sciencedirect.com/science/article/pii/S0263822317343799.

[7] Moore DT. Gradient-index optics: a review. Appl Opt 1980;19(7):1035–8. http://dx.doi.org/10.1364/AO.19.001035, URL: https://opg.optica.org/ao/abstract.cfm?uri=ao-19-7-1035, Publisher: Optica Publishing Group.

[8] Veselago VG. The electrodynamics of substances with simultaneously negative electrical and magnetic permeabilities. Sov Phys Uspekhi 1968;10:509–14. http://dx.doi.org/10.1070/PU1968v010n04ABEH003699, URL: https://ui.adsabs.harvard.edu/abs/1968SvPhU..10..509V.

[9] Hyun J, Choi W, Kim M. Gradient-index phononic crystals for highly dense flexural energy harvesting. Appl Phys Lett 2019;115(17):173901. http://dx.doi.org/10.1063/1.5111566.

[10] Zareei A, Darabi A, Leamy MJ, Alam M-R. Continuous profile flexural GRIN lens: Focusing and harvesting flexural waves. Appl Phys Lett 2018;112(2):023901. http://dx.doi.org/10.1063/1.5008576.

[11] Tol S, Degertekin FL, Erturk A. Gradient-index phononic crystal lens-based enhancement of elastic wave energy harvesting. Appl Phys Lett 2016;109(6):063902. http://dx.doi.org/10.1063/1.4960792.

[12] Zhao L, Conlon SC, Semperlotti F. An experimental study of vibration based energy harvesting in dynamically tailored structures with embedded acoustic black holes. Smart Mater Struct 2015;24(6):065039. http://dx.doi.org/10.1088/0964-1726/24/6/065039, Publisher: IOP Publishing.

[13] Sadoulet-Reboul E, Matten G, Yi K, Ouisse M. Passive discrete lens for broadband elastic guided wave focusing. J Theor Comput Appl Mech 2021;6652. http://dx.doi.org/10.46298/jtcam.6652, URL: https://jtcam.episciences.org/6652.

[14] Climente A, Torrent D, Sánchez-Dehesa J. Gradient index lenses for flexural waves based on thickness variations. Appl Phys Lett 2014;105(6):064101. http://dx.doi.org/10.1063/1.4893153.

[15] Zhao J, Cui X, Bonello B, Djafari-Rouhani B, Yuan W, Pan Y, Ren J, Zhang X, Zhong Z. Broadband sub-diffraction and ultra-high energy density focusing of elastic waves in planar gradient-index lenses. J Mech Phys Solids 2021;150:104357. http://dx.doi.org/10.1016/j.jmps.2021.104357, URL: https://www.sciencedirect.com/science/article/pii/S0022509621000545.

[16] Yi K, Collet M, Ichchou M, Li L. Flexural waves focusing through shunted piezoelectric patches. Smart Mater Struct 2016;25(7):075007. http://dx.doi.org/10.1088/0964-1726/25/7/075007, Publisher: IOP Publishing.

[17] Xu J, Li S, Tang J. In: Park G, editor. Adaptive GRIN lens based on piezoelectric metamaterial for acoustic beam focusing. Portland, Oregon, United States; 2017, 101641S. http://dx.doi.org/10.1117/12.2260341, URL: http://proceedings.spiedigitallibrary.org/proceeding.aspx?doi=10.1117/12.2260341.

[18] Lee G, Lee D, Park J, Jang Y, Kim M, Rho J. Piezoelectric energy harvesting using mechanical metamaterials and phononic crystals. Commun Phys 2022;5(1):1–16. http://dx.doi.org/10.1038/s42005-022-00869-4, URL: https://www.nature.com/articles/s42005-022-00869-4, Publisher: Nature Publishing Group.

[19] Chiou M-J, Lin Y-C, Ono T, Esashi M, Yeh S-L, Wu T-T. Focusing and waveguiding of Lamb waves in micro-fabricated piezoelectric phononic plates. Ultrason 2014;54(7):1984–90. http://dx.doi.org/10.1016/j.ultras.2014.05.007, URL: https://www.sciencedirect.com/science/article/pii/S0041624X14001255.

[20] Deng K, Ding Y, He Z, Zhao H, Shi J, Liu Z. Graded negative index lens with designable focal length by phononic crystal. J Phys D: Appl Phys 2009;42(18):185505. http://dx.doi.org/10.1088/0022-3727/42/18/185505.

[21] Hyun J, Kim M, Choi W. Partitioned gradient-index phononic crystals for full phase control. Sci Rep 2020;10(1):14630. http://dx.doi.org/10.1038/s41598-020-71397-w, URL: https://www.nature.com/articles/s41598-020-71397-w, Publisher: Nature Publishing Group.

[22] Jin Y, Torrent D, Pennec Y, Pan Y, Djafari-Rouhani B. Simultaneous control of the S and A Lamb modes by graded phononic crystal plates. J Appl Phys 2015;117(24):244904. http://dx.doi.org/10.1063/1.4923040.

[23] Kurt H, Colak E, Cakmak O, Caglayan H, Ozbay E. The focusing effect of graded index photonic crystals. Appl Phys Lett 2008;93(17):171108. http://dx.doi.org/10.1063/1.3009965.

[24] Lin S-CS, Huang TJ, Sun J-H, Wu T-T. Gradient-index phononic crystals. Phys Rev B 2009;79(9):094302. http://dx.doi.org/10.1103/PhysRevB.79.094302, URL: https://link.aps.org/doi/10.1103/PhysRevB.79.094302, Publisher: American Physical Society.

[25] Peng S, He Z, Jia H, Zhang A, Qiu C, Ke M, Liu Z. Acoustic far-field focusing effect for two-dimensional graded negative refractive-index sonic crystals. Appl Phys Lett 2010;96(26):263502. http://dx.doi.org/10.1063/1.3457447.

[26] Sukhovich A, Jing L, Page JH. Negative refraction and focusing of ultrasound in two-dimensional phononic crystals. Phys Rev B 2008;77(1):014301. http://dx.doi.org/10.1103/PhysRevB.77.014301, URL: https://link.aps.org/doi/10.1103/PhysRevB.77.014301, Publisher: American Physical Society.

[27] Tol S, Degertekin FL, Erturk A. 3D-printed phononic crystal lens for elastic wave focusing and energy harvesting. Addit Manuf 2019;29:100780. http://dx.doi.org/10.1016/j.addma.2019.100780, URL: https://www.sciencedirect.com/science/article/pii/S2214860418307188.

[28] Tol S, Degertekin FL, Erturk A. Structurally embedded reflectors and mirrors for elastic wave focusing and energy harvesting. J Appl Phys 2017;122(16):164503. http://dx.doi.org/10.1063/1.5008724, URL: https://pubs.aip.org/jap/article/122/16/164503/149586/Structurally-embedded-reflectors-and-mirrors-for.

[29] Wu T-T, Chiou M-J, Lin Y-C, Ono T. Design and fabrication of a gradient-index phononic quartz plate lens. In: Photonic and phononic properties of engineered nanostructures IV. vol. 8994, SPIE; 2014, p. 36–41. http://dx.doi.org/10.1117/12.2047881, URL: https://www.spiedigitallibrary.org/conference-proceedings-of-spie/8994/89940G/Design-and-fabrication-of-a-gradient-index-phononic-quartz-plate/10.1117/12.2047881.full.

[30] Wu T-T, Chen Y-T, Sun J-H, Lin S-CS, Huang TJ. Focusing of the lowest antisymmetric Lamb wave in a gradient-index phononic crystal plate. Appl Phys Lett 2011;98(17):171911. http://dx.doi.org/10.1063/1.3583660, URL: https://pubs.aip.org/apl/article/98/17/171911/908411/Focusing-of-the-lowest-antisymmetric-Lamb-wave-in.

[31] Yan X, Zhu R, Huang G, Yuan F-G. Focusing guided waves using surface bonded elastic metamaterials. Appl Phys Lett 2013;103(12):121901. http://dx.doi.org/10.1063/1.4821258.

[32] Zhao J, Marchal R, Bonello B, Boyko O. Efficient focalization of antisymmetric Lamb waves in gradient-index phononic crystal plates. Appl Phys Lett 2012;101(26):261905. http://dx.doi.org/10.1063/1.4773369.

[33] Zhu H, Semperlotti F. Two-dimensional structure-embedded acoustic lenses based on periodic acoustic black holes. J Appl Phys 2017;122(6):065104. http://dx.doi.org/10.1063/1.4998524, URL: https://pubs.aip.org/jap/article/122/6/065104/154730/Two-dimensional-structure-embedded-acoustic-lenses.

[34] Jiao J, Chen T, Yu D. Observation of topological valley waveguide transport of elastic waves in snowflake plates. Compos Struct 2022;286:115297. http://dx.doi.org/10.1016/j.compstruct.2022.115297, URL: https://www.sciencedirect.com/science/article/pii/S0263822322001064.

[35] Cui X, Zhao J, Boyko O, Bonello B, Zhong Z. Multi-branch subwavelength focusing of the lowest-order antisymmetric Lamb mode in a gradient-index phononic crystal. Int J Mech Sci 2019;157–158:677–83. http://dx.doi.org/10.1016/j.ijmecsci.2019.05.018, URL: https://www.sciencedirect.com/science/article/pii/S0020740319304163.

[36] Danawe H, Ozevin D, Tol S. Structurally embedded gradient index lens for guided wave amplification in polymers. Compos Struct 2024;331:117868. http://dx.doi.org/10.1016/j.compstruct.2023.117868, URL: https://www.sciencedirect.com/science/article/pii/S026382232301214X.

[37] Krpensky A, Bednarik M. Exact analytical solution for shear horizontal wave propagation through locally periodic structures realized by viscoelastic functionally graded materials. Compos Struct 2023;324:117539. http://dx.doi.org/10.1016/j.compstruct.2023.117539, URL: https://www.sciencedirect.com/science/article/pii/S0263822323008851.

[38] Zhao J, Bonello B, Boyko O. Focusing of the lowest-order antisymmetric Lamb mode behind a gradient-index acoustic metalens with local resonators. Phys Rev B 2016;93(17):174306. http://dx.doi.org/10.1103/PhysRevB.93.174306, URL: https://link.aps.org/doi/10.1103/PhysRevB.93.174306, Publisher: American Physical Society.

[39] Gao W, Hu J, Qin Z, Chu F. Flexural wave manipulation in perforated metamaterial plates with acoustic black holes interconnected by piezoelectric studs. Compos Struct 2023;321:117224. http://dx.doi.org/10.1016/j.compstruct.2023.117224, URL: https://www.sciencedirect.com/science/article/pii/S0263822323005688.

[40] Carrara M, Cacan MR, Toussaint J, Leamy MJ, Ruzzene M, Erturk A. Metamaterial-inspired structures and concepts for elastoacoustic wave energy harvesting. Smart Mater Struct 2013;22(6):065004. http://dx.doi.org/10.1088/0964-1726/22/6/065004, Publisher: IOP Publishing.

[41] Carrara M, Kulpe JA, Leadenham S, Leamy MJ, Erturk A. Fourier transform-based design of a patterned piezoelectric energy harvester integrated with an elastoacoustic mirror. Appl Phys Lett 2015;106(1):013907. http://dx.doi.org/10.1063/1.4905509.

[42] Gomez-reino C, Perez MV, Bao C, Flores-arias MT, Vidal S. Diffraction-free and diffraction-limited propagation of light in graded-index planar waveguides with hyperbolic secant refractive index profile. J Modern Opt 2000;47(1):91–102. http://dx.doi.org/10.1080/09500340008231408, URL: https://www.tandfonline.com/doi/abs/10.1080/09500340008231408, Publisher: Taylor & Francis.

[43] Timošenko SP, Woinowsky-Krieger S. Theory of plates and shells, 2. ed., [Nachdr.] ed.. McGraw-Hill classic textbook reissue, New York: McGraw-Hill; 1996.

[44] Gay D. Composite materials: Design and applications. 4th ed.. Taylor & Francis Group: CRC Press; 2023, http://dx.doi.org/10.1201/9781003195788.

[45] ISO 10352. Fibre-reinforced plastics - Moulding compounds and prepregs - Determination of mass per unit area and fibre mass per unit area. 2020.

[46] COMSOL AB, Stockholm, Sweden. COMSOL Multiphysics® v. 6.1. 2023, URL: www.comsol.co.

[47] Berenger J-P. A perfectly matched layer for the absorption of electromagnetic waves. J Comput Phys 1994;114(2):185–200. http://dx.doi.org/10.1006/jcph.1994.1159.

[48] Dubois M, Farhat M, Bossy E, Enoch S, Guenneau S, Sebbah P. Flat lens for pulse focusing of elastic waves in thin plates. Appl Phys Lett 2013;103(7):071915. http://dx.doi.org/10.1063/1.4818716, URL: https://hal.univ-antilles.fr/hal-01680699.

[49] Meyer Y, Lachat R. Vibration characterization procedure of piezoelectric ceramic parameters - Application to low-cost thin disks made of piezoceramics. MATEC Web Conf 2015;20:01003. http://dx.doi.org/10.1051/matecconf/20152001003, URL: https://www.matec-conferences.org/articles/matecconf/abs/2015/01/matecconf_ave2014_01003/matecconf_ave2014_01003.html, Publisher: EDP Sciences.

[50] Meirovitch L. Fundamentals of vibration. Mcgraw-Hill Publ.Comp.; 2003.